Astronomy Letters, vol. 30, No.1, 2004 February 2, 2008
Translated from Pis'ma v Astronomicheskii Zhurnal, vol.30, No.1, 2004, pp. 3-16

The phenomenon of the galaxy NGC 6286: a forming polar ring or a superwind?

L.V. Shalyapina[1], A.V. Moiseev[2], V.A.Yakovleva[1], V.A. Hagen-Thorn[1], and A. N. Burenkov[2]

[1] Astronomical Institute, St. Petersburg State University, Universitetsky pr.28, Petrodvorets, 198504 Russia
[2] Special Astrophysical Observatory, Russian Academy of Sciences, Nizhnii Arkhyz, Karachai-Cherkessian Republic, 357147 Russia

Received March 20, 2003

Abstract. We present the observations of the pair of interacting galaxies NGC6285/86 carried out with the 6m Special Astrophysical Observatory (SAO) telescope by using 1D and 2D spectroscopy. The observations of NGC6286 with a long-slit spectrograph (UAGS) near the H_α line revealed the rotation of the gaseous disk around an axis offset by $5'' - 7''$ from the photometric center and a luminous gas at a distance up to 9 kpc in a direction perpendicular to the galactic plane. Using a multipupil fiber spectrograph (MPFS), we constructed the velocity fields of the stellar and gaseous components in the central region of this galaxy, which proved to be similar. The similar line-of-sight velocities of the pair and the wide ($5' \times 5'$) field of view of the scanning Fabry-Perot interferometer (IFP) allowed us to obtain images in the H_α and [NII] λ6583 emission lines and in the continuum as well as to construct the line-of-sight velocity fields and to map the distribution of the [NII]λ6583/H_α ratio for both galaxies simultaneously. Based on these data, we studied the gas kinematics in the galaxies, constructed their rotation curves, and estimated their masses ($2{\cdot}10^{11} M_\odot$ for NGC6286 and $1.2{\cdot}10^{10}\ M_\odot$ for NGC6285). We found no evidence of gas rotation around the major axis of NGC6286, which argues against the assumption that this galaxy has a forming polar ring. The IFP observations revealed an emission nebula around this galaxy with a structure characteristic for superwind galaxies. The large [NII]λ6583/H_α ratio, which suggests the collisional excitation of its emission, and the high infrared luminosity are additional arguments for the hypothesis of a superwind in the galaxy NGC 6286. A close encounter of the two galaxies was probably responsible for the starburst and the bipolar outflow of hot gas from the central region of the disk

INTRODUCTION

NGC6285/86 (Arp 293) is a pair of interacting galaxies (Fig. 1) with similar luminosities and radial velocities[1]. They are $\sim 1\farcm5$ apart, which corresponds to ~ 40 kpc for a distance $D = 91$ Mpc (at $H_0 = 65\,\mathrm{km\,s^{-1}}\,Mpc$ and $V_{sys}^{gal} = 5925\,\mathrm{km\,s^{-1}}$; see below). A faint 'bridge' can be seen between the galaxies in deep CCD images. Whitmore et al. (1990) included one of the galaxies from the pair, NGC6286, in the catalog of polar-ring galaxies as a possible candidate (C51), because a diffuse structure (semi-ring) located to the SE of the main body of the galaxy is clearly seen in the reproduction in the atlas by Arp (1966).

NGC6286 is a spiral Sb-type (RC3) galaxy seen almost edge-on with a thick dust lane that runs inclined to the stellar disk of the galaxy. Since, according to IRAS data, this galaxy has a high infrared luminosity, $\log(L_{FIR}/L_B) = 11.28$ (Soifer et al. 1987), it was included in the studies of bright infrared galaxies (see, e.g., Baan 1989; Young et al. 1989). The infrared fluxes from NGC6286 were measured at various wavelengths (Soifer et al. 1987, 1989). These fluxes were used to determine the dust temperature and mass (Young et al. 1989) and to estimate the star-formation rate, $SFR = 56\,M_\odot\,yr^{-1}$ (Smith et al. 1998). Based on radio data, Sanders et al. (1986) estimated the H2 mass for this galaxy, $\log M(H_2)/M_\odot = 9.97$.

The optical spectra of this galaxy were described by several authors. Reshetnikov & Combes (1994) classified its nuclear spectrum as H II and pointed out a peculiarity in the radial velocity distribution of the gas along the minor axis of the galaxy. Veilleux et al. (1995) classified the nuclear spectra of NGC6286 and NGC6285 as LINER and H II, respectively. Smith et al. (1996) used the H_α line measurements to construct the rotation curve for NGC6286 and estimated its mass ($M = 1.3 \cdot 10^{11} M_\odot$). Reshetnikov et al. (1996) performed a detailed photometric study of NGC6286 in the B, V, R_C bands. Based on peculiarities of the line-of-sight velocity curve along its minor axis and on photometric data, they assumed that the diffuse structure (semi-ring) located at the SE edge of the galaxy is a forming polar ring. To analyze the kine-

Send offprint requests to: L.V. Shalyapina, e-mail: lshal@astro.spbu.ru

[1] According to NED data

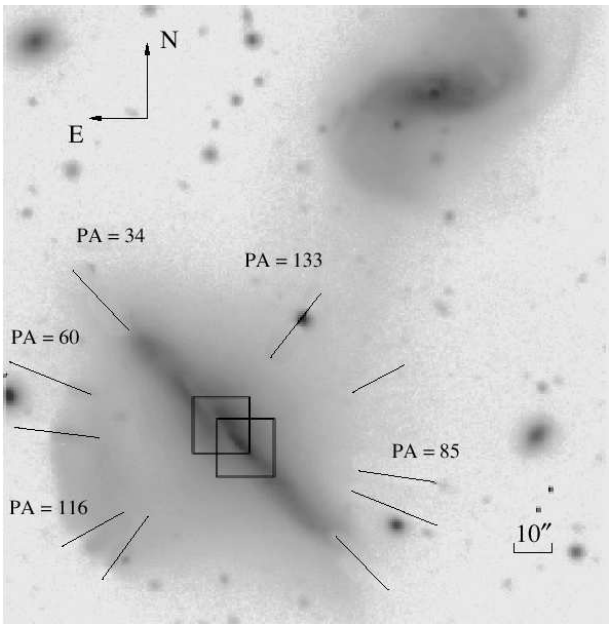

Fig. 1. Fig. 1. The R_C-band image of the NGC6285/86 pair obtained with the 6-m SAO telescope (for the assumed distance to the galaxies of $D = 91$ Mpc; $1''$ corresponds to 0.44 kpc).

matics of the gaseous and stellar components of the galaxy NGC6286 in more detail, we have undertaken its study by using long-slit (1D) and 2D (panoramic) spectroscopy.

1. OBSERVATIONS AND DATA REDUCTION

The spectroscopic observations of NGC6286 were performed at the prime focus of the 6-m SAO telescope. The first observations were carried out with the long-slit spectrograph UAGS (Afanasiev et al. 1995) in 1997 and 1999. The observations with the multipupil fiber spectrograph MPFS (Afanasiev et al. 2001; a description of the spectrograph can be found on the Internet at the SAO WWW page[2]) were performed in 2001, and the data with a scanning Fabry-Perot interferometer (IFP) were obtained in 2002. A log of observations is given in Table 1.

In UAGS, the detectors were Electron 530×580 - pixels and Photometrics 1024×1024-pixel CCDs in 1997 and 1999, respectively. The UAGS slit size was $2'' \times 140''$. The observed spectral range included the H_α, [NII]λ6548, 6583 and [SII]λ6716, 6731 emission lines.

The UAGS spectral data were reduced in the ESO-MIDAS environment using the LONG subroutine. After the primary reductions, we performed a smoothing along the slit with windows of $0''.8$ for the central region and $2''$ starting from a distance of $15''$ from the center. The line-of-sight velocities were measured from the positions of the centers of the Gaussians fitted to the emission lines. The accuracy of these measurements was estimated from the nightsky [OI]λ6300 line to be $\pm10\,\mathrm{km\,s^{-1}}$. We also measured the relative intensities and $FWHM$s of the emission lines. The observed $FWHM$s were corrected for the width of the instrumental profile by using the standard relation $(FWHM)^2 = (FWHM)^2_{obs} + (FWHM)^2_{instr}$. According to the measurements of lines from a calibration lamp, the $FWHM$ of the instrumental profile was 3.6 Å. The H_α, [NII]λ6583, and [SII]λ6716, 6731 emission lines are most intense in the spectrum of this galaxy. These lines were used to construct the line-of-sight velocity curves for the ionized gas.

During our MPFS observations, we took spectra from 240 spatial elements (in the form of square lenses) simultaneously that formed an array of 16×15 elements in the plane of the sky. The angular size of a single element was $1''$. The detector was a Techtronix 1024×1024 - pixels CCD. The observations were carried out in two spectral ranges. The green range included emission lines of the gaseous component (H_β, [OIII]λ4959, 5007) and absorption features of the stellar population of the galaxy (MgIλ5175, FeIλ5229, FeI + CaIλ5270, etc.). The red range contained the H_α, [NII]λ6548, 6583, and [SII]λ6716, 6730 emission lines.

We reduced the observations by using the software that was developed by V.L. Afanasiev (SAO) and that runs in the IDL environment. We constructed two-dimensional maps of the emission lines intensities and ionized gas line-of-sight velocity fields by using Gaussian fitting of the emission lines profiles. The line-of-sight velocities were determined with an accuracy of $10-15\,\mathrm{km\,s^{-1}}$. The line-of-sight velocity fields of the stellar component were constructed by means of a cross-correlation technique modified for 2D spectroscopic data and described by Moiseev (2001). Spectra of the star HD 148293 and the twilight sky were used as templates for cross-correlation. The line-of-sight velocities were determined from the absorption lines with an accuracy of $\sim 10\,\mathrm{km\,s^{-1}}$.

The IFP observations were carried out by using the SCORPIO multi-mode focal reducer. The reducer is described at the SAO WWW-page[3] its parameters in interferometric observations were given by Moiseev (2002).

For our observations, we used the interferometer in the 235th order at a wavelength of 6562.8 Å. The interfringe $\Delta\lambda = 28$Å corresponded to a $\sim 1270\,\mathrm{km\,s^{-1}}$ range free from orders overlapping. Premonochromatization was made by using narrow-band filters with $FWHM = 19-20$Å centered at the spectral range included the H_α or [NII]λ6583 emission lines of the galaxy. During an exposure, we sequentially took 32 interferograms of the object at various IFP's gaps, the size of the spectral channel was about 0.9 Å ($\sim 40\,\mathrm{km\,s^{-1}}$). The width of the instrumental profile was $FWHM = 2.5$Å ($\sim 110\,\mathrm{km\,s^{-1}}$). The detector was the same CCD as in the MPFS observations. Since the readout was performed with 2×2 binning, a 512×512-pixel image (the pixel size was $0''.56$) was obtained in each spectral channel.

We reduced the interferometric data by using the IDL-based software developed at the SAO (Moiseev 2002).

[2] http://www.sao.ru/hq/lsfvo/devices.html

[3] http://www.sao.ru/hq/moisav/scorpio/scorpio.html

Table 1. A log of observations

Instrument, year	Exposure time s	PA, field	Spectral range Å	Reciprocal dispersion Å/px	Seeing
UAGS	3×1800	34°	6200-7000	1.5	$3''.2$
Sep. 1997	3×1800	116°	6200-7000	1.5	$2''.5$
	3×1800	133°	6200-7000	1.5	$2''.5$
UAGS	3×1800	60°	6200-7000	1.2	$1''.6$
Aug.-Sep. 1999	3×1800	85°	6200-7000	1.2	$1''.6$
	3×1800	85°	6200-7000	1.2	$1''.5$
	3×1800	133°	6200-7000	1.2	$1''.6$
MPFS	3×1200	Center	4900-6200	1.4	$2''.0$
Apr.-Sep. 2001	3×900	Center	5900-7200	1.4	$2 - 2.5''$
IFP	32×300		H_α + [NII]	0.9	$1''.5$
Apr.-Sep 2002	32×180		[NII]λ6583	0.9	$2''.0$

After the preliminary reduction (a subtraction of night-sky lines and wavelength calibration), the observational data were collected to data cubes where each point in a 512×512 field contained a 32-channel spectrum. A Gaussian smoothing along a spectral domain with $FWHM = 1.5$ channels and a two-dimensional Gaussian smoothing in a spatial domain with $FWHM = 2 - 3$ pixels (depending on the seeing), was made by using the ADHOC package[4]. To construct the velocity fields and monochromatic images, we fitted the emission line profiles by Gaussians. The measurement errors of the line-of-sight velocities did not exceed $10\,\mathrm{km\,s^{-1}}$ for single lines.

However, the following factor hindered our measurements of the line-of-sight velocities and intensities of the emission lines during our observations near H_α. According to the long-slit observations, the range of line-of-sight velocities in the galactic disk is $450-500\,\mathrm{km\,s^{-1}}$ (see below). On the wavelength scale, this range accounted for about half of the $FWHM$ of the narrow-band filter used to separate the desired spectral range (see Fig. 2 top). Therefore, during the observations with the IFP670 filter centered on the shifted H_α line ($\lambda_C = 6691$Å), the [NII]λ6583 line was also seen in the wing of the filter transmission curve in the central and SW regions of the galaxy. Thus, for the blueshifted regions, the observed intensity of the nitrogen line increased sharply, while the intensity of the H_α line decreased. Our standard procedure of the correction for the filter transmission curve ("a spectral flat-field") does not allow the true intensities of the lines in the wing of the filter transmission curve to be restored (Moiseev 2002). In addition, in the central region of the galaxy (see Section 2.1), the H_α and [NII] line IFP-profiles slightly overlap because the $FWHMs$ of the emission lines increase. The both effects (the increases in relative [NII] intensity and line profile width) made it difficult to measure the line-of-sight velocities and intensities of H_α in the central and SW regions of the galactic disk.

To improve the line-of-sight velocities in the galactic disk, we carried out additional observations with a fil-

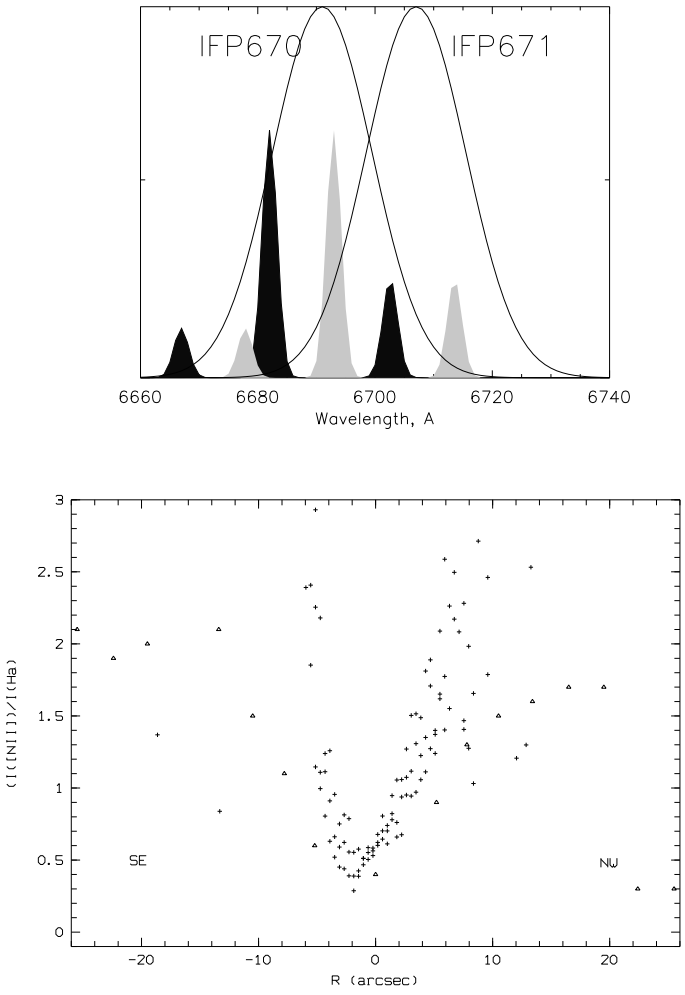

Fig. 2. (top) IFP observations. The spectra of the galaxy (the H_α and NII]λ6548, λ6583 lines) are shown schematically. The spectra that correspond to $V = 5450$ and $5950\,\mathrm{km\,s^{-1}}$ are colored black and gray, respectively. The solid lines represent the transmission curves of both filters (IFP670 and IFP671). (bottom) The distribution of the [NII]λ6583/H_α ratio, as constructed from UAGS (crosses) and IFP (triangles) data (at $PA = 116°$).

[4] The ADHOC software package was developed by J. Boulesteix (the Marseilles Observatory) and is freely available on the Internet.

ter centered on the [NII]λ6583 line (IFP671 with λ_C = 6707Å). In this case, the filter separated only one spectral line (Fig. 2top).

Thus, we constructed the line-of-sight velocity fields and intensity distributions in the H_α and [NII]λ6583 lines from the observations with IFP670 and IFP671, respectively. A comparison of the measured line intensities based on the UAGS and IFP observations shows a good agreement (Fig. 2 bottom). We also mapped the galaxies in the continuum near the emission lines.

2. RESULTS

2.1. UAGS spectra

We have obtained long-slit spectra of NGC6286 near H_α at the five position angles of the slit which are marked on the Fig. 1. The line-of-sight velocities were measured from the H_α, [NII]λ6548, 6583 and [SII]λ6716, 6730 emission lines. The data obtained from the forbidden lines are in close agreement, within the errors. However, since [NII]λ6583 is more intense than the other lines, we will present the measurements of this line only. Below, we give heliocentric velocities.

Figure 3a shows the line-of-sight velocity distribution along the major axis ($PA = 34°$). On the horizontal axis, $R = 0$ corresponds to the position of the peak continuum intensity (the photometric center). In most of the velocity curve, the line-of-sight velocities measured from both lines (H_α, [NII]) are equal, except the region $-9'' < R < 7''$ where the data obtained from these lines systematically differ by $\sim 20\,\mathrm{km\,s^{-1}}$.

The line-of-sight velocity to the SW from the photometric center is almost constant, slightly decreasing toward the galactic edge. In the region $0 < R < 6''$, the line-of-sight velocity gradient is roughly constant. In the NE direction the velocity increases, but with a slightly smaller gradient. Note that the slit crosses the dust lane here. At distances from the photometric center larger than $22''$, the curve flattens out, as confirmed by the data obtained later with the IFP.

Since the galaxy is seen nearly edge-on, the line-of-sight velocity curve along its major axis may be considered to be the curve of circular rotation (to within the line-of-sight projection of the non-circular velocities). Within the errors, our data closely agree with the rotation curve from Smith et al. (1996) if we take the middle point of the line-of-sight velocity range, which is offset by about $5\farcs5$ to the NE of the photometric center, as the coordinate origin and assume that the velocity at this point ($5650\,\mathrm{km\,s^{-1}}$) is the velocity of the system.

The misalignment of the photometric and dynamical centers also follows from our MPFS and IFP observations (see Sections 2.2 and 2.3) and is probably attributable to the presence of light-absorbing dust in the circumnuclear region. Note that there is a large uncertainty in establishing the position of the galaxy nucleus. Since the dust lane runs at an angle to the disk plane (Fig. 1), the isophotes shape in the central region is distorted and asymmetric (Smith et al. 1996; Reshetnikov et al., 1996). As a result, the intensity peak is shifted to the SW from the nucleus, and this shift changes with wavelength due to selective dust absorption.

The middle parts of the line-of-sight velocity curves constructed at $PA = 60°$ and $85°$ have rectilinear segments. As in the previous case, the centers of their symmetry do not coincide with the positions of the continuum intensity peaks, and the gradients decrease with increasing angle between the major axis of the galaxy and the spectrograph slit. The rectilinear segments are about $5''$ long, which suggests solid-body rotation of the gaseous galactic disk in this region. A surprising fact is that the emission lines are observed up to a distance of 4 kpc on both sides of the plane of the galactic disk.

The line-of-sight velocities at the spectrograph slit positions close to the direction of the minor axis of the galaxy are differ. At $PA = 133°$, the line-of-sight velocity is constant in the central region ($R < 5'' - 6''$), as must be the case for circular rotation of the gaseous disk in the galactic plane. Further out as one recedes from the center on both sides, there is a large spread in line-of-sight velocities, with the intensity of the [NII]λ6583 line increasing compared to the intensity of H_α. In this case, the spectrograph slit crossed the major axis of the galaxy at a point offset by $\sim 6''$ to the NE of the photometric center.

Let us consider the features of the line-of-sight velocity curve at $PA = 116°$ shown in Fig. 3b. The emission lines are traceable far from the disk plane, up to 9 kpc in the SE direction. In the central part of the curve, the line-of-sight velocities increase on both sides of the center. This behavior of the line-of-sight velocities can be explained by assuming that the directions of the slit and the rotation axis almost coincide and that the slit position is shifted by about $5'' - 7''$ to the SW from the dynamical center. This assumption is justified in Section 2.3.

Apart from the line-of-sight velocities, we measured the relative intensities and the $FWHMs$ of the emission lines. As we noted above, a characteristic feature of the individual spectra is an increase in the intensity of the [NII] line compared to the intensity of H_α as one recedes from the disk plane (Fig. 2b). The [NII]/H_α ratio is 0.35 at the photometric center and reaches 1.5 in outer galactic regions. Below (see Section 2.3), we will consider the distribution of relative line intensities in more detail by using IFP data.

The UAGS data suggest the existence of a luminous gas far from the plane of the galactic disk, but they do not allow the full picture of its motion to be constructed. In addition, they give no information about the stellar component of the galaxy. Such information was obtained when NGC6286 was studied by using 2D spectroscopy.

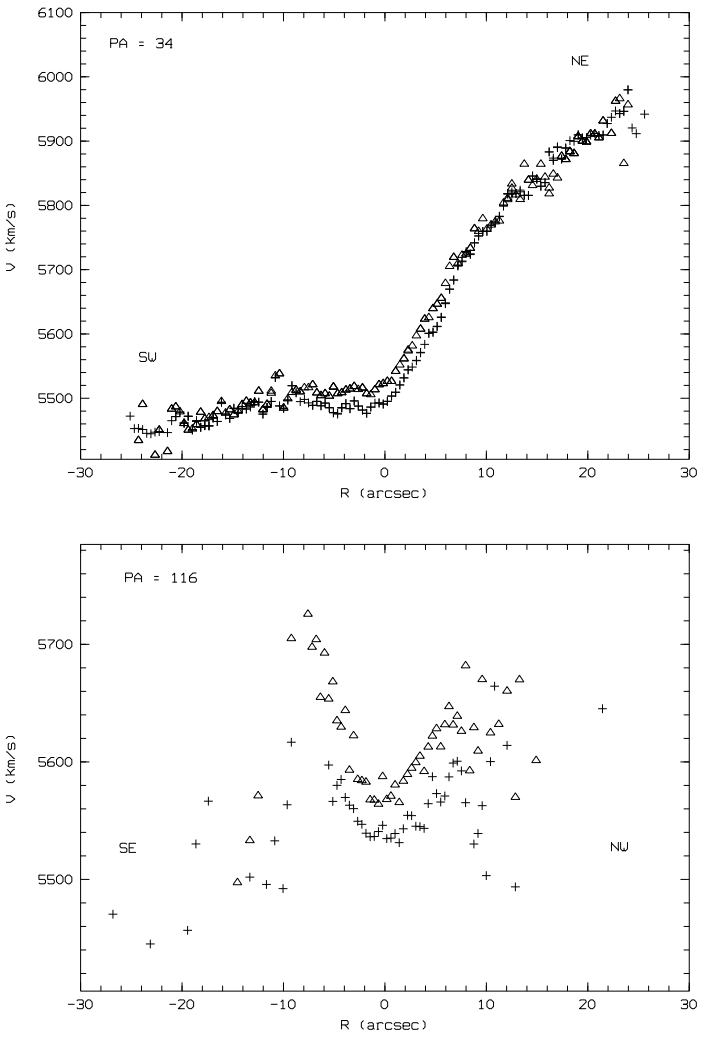

Fig. 3. Line-of-sight velocity curves: (top) $PA = 34°$ along the major axis of the galaxy, (bottom) $PA = 116°$; the crosses mark H_α measurements, and the triangles mark [NII]λ6583 ratio. The peak of a continuum intensity was taken as zero point on the horizontal axis.

2.2. MPFS spectra

The MPFS observations were performed for the central part of the galaxy. The positions of the spectrograph fields are shown in Fig. 1. The center of the fields coincide with the photometric center in the green spectral range and is shifted by $5''$ to the NE in the red range. Near and to the SW of the photometric center, the line-of-sight velocities of the forbidden lines are higher than those of H_α and H_β, as in the case of long-slit spectra. In general, however, the velocity fields constructed from the emission lines are similar, and we will consider the data obtained from H_β to compare them with the velocity field of the stellar component. The results are shown in Fig. 4. We see that the motions of the stellar and gaseous components are similar and generally consistent with the assumption of circular rotation of the gas and stars, although the isovelocities are appreciably distorted in both fields. These distortions are most likely attributable to the presence of dust. Since the size of the field of view is relatively small, we failed to determine the position of the dynamical center accurately. We may only note that it is shifted to the NE of the photometric center.

Based on the measured equivalent widths of absorption lines, we determined the chemical indices Mgb and $< Fe >$ in the Lick system (Worthey et al. 1994) and constructed their radial distributions. The indices Mgb increase from 1.8 to 3, while the indices $< Fe >$ have a small gradient and change from 1.5 to 2. The $[Mgb/ < Fe >]$ ratio changes from 0.0 dex near the photometric center to +0.3 dex at a distance of $4'' - 5''$ to the NE. Using model calculations (Worthey, 1994), we determined the mean metallicity and age of the stellar population. Unfortunately, because of the strong emission in H_β, we were unable to isolate the absorption line and made estimates by using only metal absorption lines. Hence we could not reliably separate the effects of a metallicity and age variations. Therefore, the metallicity near the photometric center of the galaxy is determined unambiguously, $[Fe/H] = 1$ dex, while the age can range from $12 \cdot 10^9\, M_\odot$ to $17 \cdot 10^9\, M_\odot$ years. At a distance of $4'' - 5''$ to the NE (in a region closer to the galactic nucleus), the metallicity and age lie within the ranges $0.0 - 0.25$ dex and $1.5 - 2 \cdot 10^9\, M_\odot$ yrs, respectively. These results provide circumstantial evidence that the galactic nucleus (where the metallicity must be higher and the age must be younger) does not coincide with the photometric center.

2.3. IFP data

The IFP observations were performed in the H_α and [NII]λ6583 lines. Since the interferometer has a large field of view, the line-of-sight velocity fields as well as the distributions of the emission lines and continuum intensities, lines' $FWHMs$, and lines ratio were constructed for both components of the interacting system NGC6285/86 (Fig. 5). As we see from this figure, both the velocity fields and the emission-line images of each component are peculiar, but the most peculiar features are observed in NGC6286. Let us consider the data for each galaxy in more detail.

2.3.1. NGC 6286

Intense emission is observed in the central part of the galactic disk, and a bright H II region can be identified at $\sim 10''$ to the SW from the photometric center. The [NII]λ6583/H_α ratio in the disk changes slightly; it is approximately equal to 0.35 in the SW part and is, on average, slightly higher in the NE part, being largest (0.6) near the dust lane. Since this ratio increases in the dust lane, we may assume that in this region we see the outer parts of the disk where the physical conditions differ from the conditions at the center. The relatively small [NII]λ6583/H_α ratio suggests that photoionization is responsible for the formation of the emission-line spectrum.

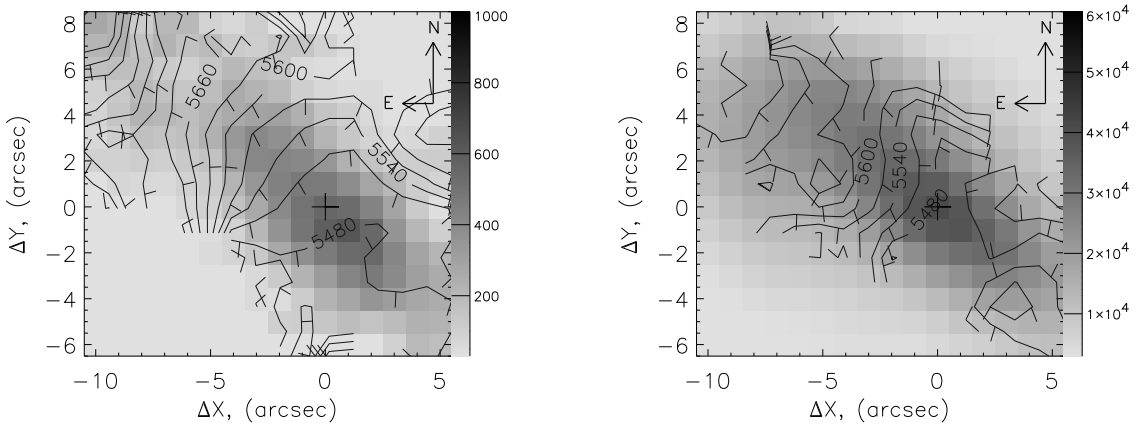

Fig. 4. MPFS data. The line-of-sight velocity fields of the gaseous component found from the H_β (left) and of stars (right) are overlapped on the H_β and continuum intensity distributions (their gray scale is in arbitrary units). The point with coordinates (0,0) corresponds to the continuum intensity peak.

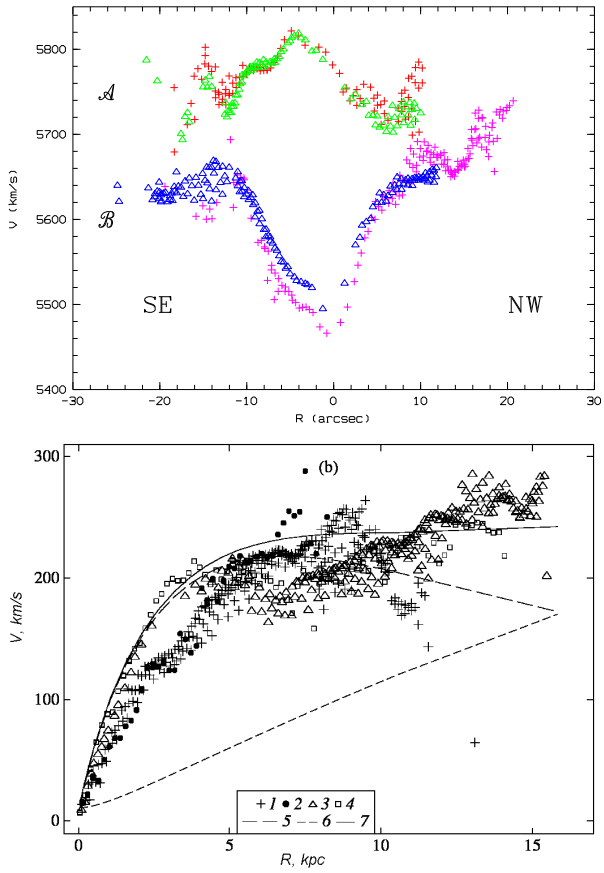

Fig. 6. (top) The line-of-sight velocity distributions in the emission-line regions A and B at slit positions parallel to the minor axis of the galaxy constructed from IFP observations: the crosses the H_α data; the triangles represent the [NII]λ6583 data. (bottom) The rotation curve for NGC6286. The NE half of the line-of-sight velocity curve: 1 and 2 represent the IFP and UAGS data, respectively; The SW half: 3 and 4 represent the IFP and UAGS data, respectively; 5 is the model rotation curve for the disk, 6 is the halo model, and 7 is the ultimate model rotation curve for NGC6286.

A comparison of Figs. 5a, 5b, and 5c shows that the emission-line and continuum intensity distributions for NGC6286 are different. In all cases, disk components crossed by the dust lane are traceable. The outer continuum isophotes are lenticular in shape, while two extended regions that are symmetric relative to the point shifted from the photometric center by about $5'' - 7''$ to the NE in the continuum are observed in the emission lines. These regions are slightly asymmetric in extent relative to the disk plane; their SE parts are slightly larger than their NW parts. Remarkably, with the exception of a few separate knots, there is no gas emission inside the cones with an opening angle of about 60° the vertices of which are located at the above point. On both sides of the plane of the galactic disk, the intensity of the [NII] lines rapidly increases compared to H_α (Fig. 5f). Along the generatrices of the cones, the line ratio reaches its maximum, [NII]/$H_\alpha = 2 - 2.5$. Figure 5d shows the distribution of $FWHMs$ for the [NII]λ6583 line. The $FWHM$ changes from ~ 200 to $\sim 320\,\mathrm{km\,s^{-1}}$ in the galactic disk and reaches its maximum, $\sim 400\,\mathrm{km\,s^{-1}}$, along the generatrices of the cones.

The emission nebula that we detected in NGC6286 (Figs. 5b and 5c) resembles in shape the nebulae observed in superwind galaxies, for example, NGC1482 (Veilleux 2002). Not only the images of both galaxies in the H_α and [NII] lines but also the distribution maps of the [NII]λ6583/H_α ratio are similar. The shape of the isovelocities near the gaseous disk is indicative of its rotation around an axis perpendicular to the galactic plane. However, this axis does not pass through the photometric center in the continuum, but is shifted by $5'' - 7''$ to the NE of it. Its position roughly coincides with the vertices of the cones in the emission-line images. The extent of the disk to the SW of the dynamical center is a factor of approximately 1.5 larger than its extent to the NE, which may be attributable to the disk asymmetry that resulted from the gravitational interaction with the companion.

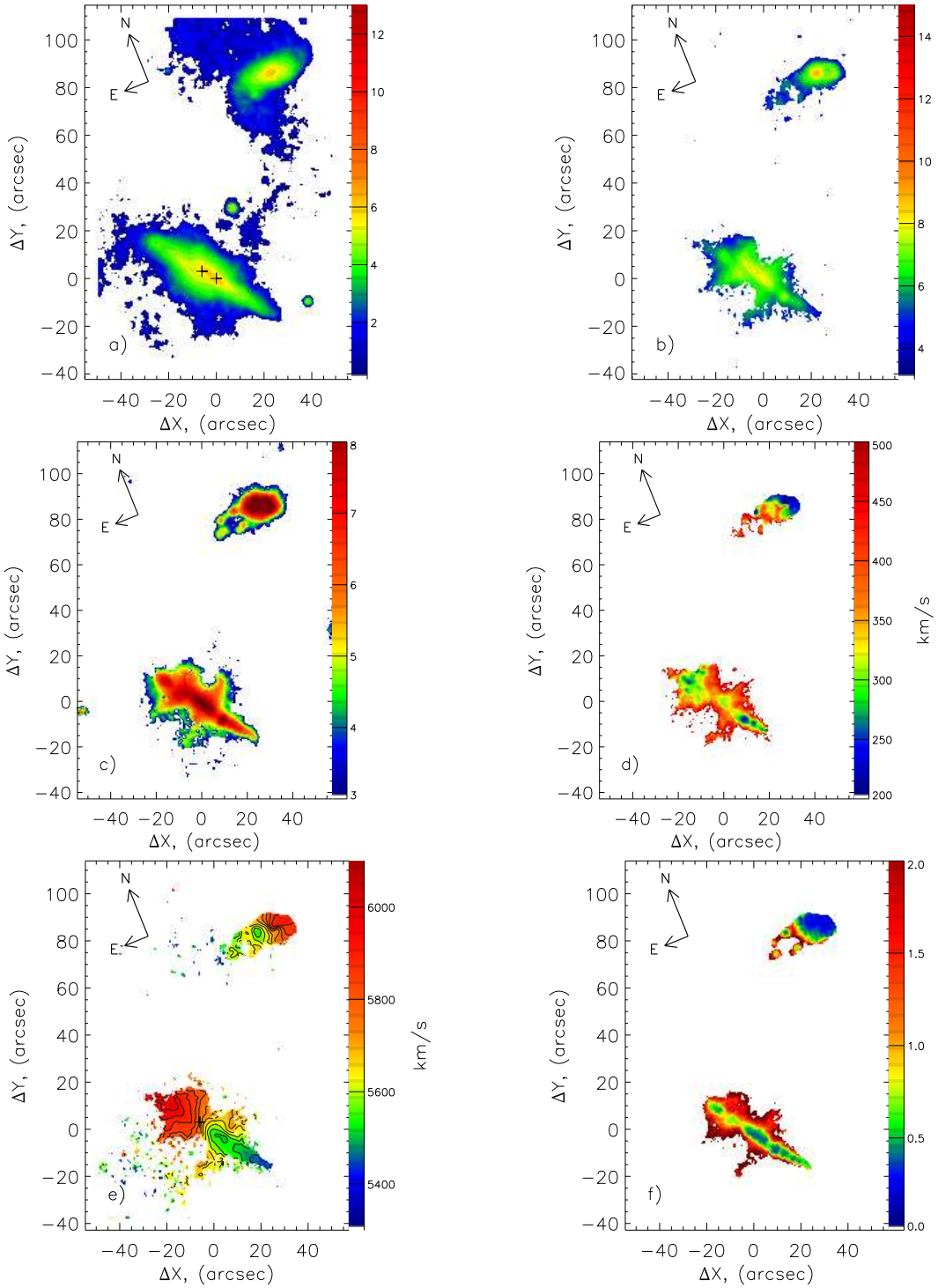

Fig. 5. IFP data: (a) the continuum intensity distribution, the crosses mark the positions of the photometric $(0, 0)$ and dynamical $(6, 3)$ centers; (b) and (c) the intensity distributions in the [NII]λ6583 and H_α lines (the gray scale is in arbitrary units); (d) the distribution of $FWHMs$ for the [NII]λ6583 line; (e) the velocity fields in this line, isovelocities are plotted in them at steps of $40\,\mathrm{km\,s^{-1}}$, the cross marks the position of the dynamical center, the velocity at this point is $5690\,\mathrm{km\,s^{-1}}$; and (f) is the [NII]$\lambda$6583/$H_\alpha$ ratio.

The shape of the isovelocities in emission-line regions outside the galactic disk (Fig. 5e) is of considerable interest. The velocities are approximately constant along the straight lines that are parallel to the generatrices of the cones. For a clearer illustration of the peculiarities of the velocity field, Fig. 6(top) shows one-dimensional line-of-sight velocity distributions in directions that are perpendicular to the disk plane and that are offset from the dynamical center by 2 kpc to the NE (profile 'A') and SW (profile 'B'). Both profiles pass through the most ex-

tended parts of the emission nebula. The line-of-sight velocity curves are symmetric relative to the disk plane and are mirror reflections relative to each other. The line-of-sight velocity amplitude in profile 'A' that passes through the dust lane is smaller than that in profile 'B'. The central parts of the profiles reflect the rotation of the gaseous disk; both profiles flatten out in the outer parts, with the mean velocities being approximately equal to 5720 and $5650\,\mathrm{km\,s^{-1}}$, respectively. As we see from the velocity field, there is no evidence of gas motion around the major axis of the galaxy.

2.3.2. NGC 6285

The emission-line intensity distribution for the companion galaxy (Fig. 5b) exhibits the following features: a gaseous disk, intense emission in the nucleus, and a bright HII region $\sim 7''$ to the west of the nucleus. The nucleus and the HII region lie on the opposite sides of the ring-like structure ($7''$ in diameter) that is clearly seen in the H_α and [NII] images. The SE side of the gaseous disk is elongated and bent toward the neighboring galaxy. In the unperturbed western part of the disk, the [NII]λ6583/H_α ratio is almost constant, being ~ 0.4, which suggests that photoionization is responsible for the formation of the emission. In the region where the disk is bent, the ratio changes randomly and, on average, is approximately equal to 1.3. Peculiar features in the line-of-sight velocity field can also be seen in this part of the disk (Fig. 5e). In general, the velocity field of NGC6285 is characteristic of an inclined gaseous disk with solid-body rotation in its central part. However, the isovelocities are distorted both at the center and on the periphery, particularly in the SE part of the galaxy.

3. ANALYSIS OF OBSERVATIONAL DATA AND DISCUSSION

3.1. The Kinematics of Gas in the Galaxies of the Pair

3.1.1. NGC 6286

Since NGC6286 is seen nearly edge-on ($i = 89°$; Smith et al. 1996), we constructed the rotation curve for this galaxy from our line-of-sight velocity measurements of the H_α and [NII] lines along its major axis by using both long-slit spectra and IFP data. The direction of the rotation axis and the position of the dynamical center were determined from the velocity field (Fig. 5e). Subsequently, we improved this position by achieving the closest coincidence in the region where the gradient of both halves of the line-of-sight velocity curve reached a maximum and where the latter flattened out. As a result, we obtained $V_{hel}^{sys} = 5690 \pm 10\,\mathrm{km\,s^{-1}}$ for the heliocentric velocity of the galaxy, which yields $V_{gal}^{sys} = 5925\,\mathrm{km\,s^{-1}}$.

Figure 6(bottom) shows the rotation curve on which the data for the two halves of the line-of-sight velocity curve are plotted by different symbols. Apart from the central region, $R \leq 1$ kpc, there is good agreement between the SW and NE parts of the curve only in some segments. Some differences between the two parts of the curve can be easily explained. For example, the decrease in velocity at $1.5 \leq R \leq 4.5$ kpc in the NE part of the curve stems from the fact that the dust lane passes through this region. Dust to decrease the velocity in the rotation curves of disk galaxies seen almost edge-on (Bosma et al. 1992) . The thickest part of the dust lane ends at a distance $R \sim 5$ kpc, and both branches of the rotation curve converge. Further out, we see a local minimum of the line-of-sight velocity on the SW branch at $5.5 \leq R \leq 7.5$ kpc. The giant H II region mentioned in Section 2.3, which probably has local non-circular motions, is located precisely in this place. Note that the waves in the line-of-sight velocity curves caused by various factors are a common phenomenon.

The initial part of the rotation curve, up to $R \sim 5$ kpc along the SW half, is well fitted by the model curve (Monnet & Simien 1977) that corresponds to the rotation of an exponential disk with a scale factor $h = 3$ kpc (the curve plotted by long dashes in Fig. 6bottom). However, at a distance $R \geq 5$ kpc, the points lie above this curve. Therefore, we must assume the existence of a spherical isothermal halo to represent the observed curve over its entire length. Calculations show that this halo must have the following parameters: the central density is $\rho_0 = 0.017\,M_\odot\,pc^3$ and the core radius is $r_c = 84$ kpc (Fig. 6, short dashes). The ultimate theoretical rotation curve is represented by the solid line in Fig. 6b. This curve exhibits a rapid rise up to $R \sim 5$ kpc, which then slows down; the velocity reaches $V = 240\,\mathrm{km\,s^{-1}}$ at $R \sim 8$ kpc, which yields an estimate of the mass within this radius, $1.1 \cdot 10^{11}\,M_\odot$. The total mass of the galaxy with the halo is $2 \cdot 10^{11}\,M_\odot$.

We particularly emphasize that we have found no spectroscopic evidence for the existence of a kinematically decoupled system that rotates in the polar plane with respect to the galactic disk. The line-of-sight velocity distributions shown in Figs. 5e and 6(top) indicate that in regions far from the disk plane, the velocities are close to the velocity of the galactic center; i.e., they correspond to those that might be expected in a spherically symmetric halo.

3.1.2. NGC 6285

As we noted above (Section 2.3), the velocity field of the companion galaxy NGC6285 generally corresponds to the rotation of an inclined gaseous disk. We fitted our data by the model of gas rotation in circular orbits with the following parameters: the heliocentric line-of-sight velocity of the dynamical center is $5670\,\mathrm{km\,s^{-1}}$ ($V_{gal}^{sys} = 5905\,\mathrm{km\,s^{-1}}$) and the inclination of the disk plane to the plane of the sky is $i \sim 60°$. The velocity turned out to reach its maximum, $184\,\mathrm{km\,s^{-1}}$, at a distance of ~ 4 kpc. The mass within the radius of 2 kpc is $10^{10}\,M_\odot$. Regions with high residual velocities ($\pm 50\,\mathrm{km\,s^{-1}}$) can be identified in the

region of the ring-like structure between the nucleus and the bright H II region and on the SE side of the disk where the isovelocities are distorted. The high residual velocities are indicative of appreciable non-circular motions in these regions.

3.2. The Superwind in NGC6286

Both the photometric and spectroscopic data suggest that NGC6285/86 is a pair of interacting galaxies. The strong interaction between them is evidenced by the distortions of the structure of the galaxies – the asymmetry of their gaseous disks and the inclined dust lane in NGC6286; the existence of a bridge between the galaxies and an extended luminous region to the SE of NGC6285; and peculiarities of the velocity fields. The most probable range of relative space velocities of the galaxies during their close encounter is $50-100\,\mathrm{km\,s^{-1}}$. The probability that their relative space velocity is outside this range for the derived line-of-sight velocity difference between the galaxies of $\sim 20\,\mathrm{km\,s^{-1}}$ is low. We can then estimate the characteristic interaction time, about 10^8 yrs.

The interaction during a close passage of the galaxies could trigger a strong starburst in the central part of NGC6286. This conclusion is confirmed by FIR and IR data, according to which NGC6285 is a galaxy with a high FIR luminosity: $\log(L_{FIR}/L_\odot) = 11.28$. Such a luminosity L_{FIR} is suggestive of a high star-formation rate: $56 - 65\,M_\odot\,yr^{-1}$ (Smith et al. 1998; Poggianti & Wu, 2000).

This a high rate of star formation, which, in addition, takes place in a relatively small region in the central part of the galaxy, eventually leads to a much higher supernova rate than that in normal spiral galaxies. As a result, a phenomenon called a superwind will be arised (Heckman et al. 1990). This phenomenon consists in the strong heating of the interstellar medium and its outflow in a direction perpendicular to the galactic disk. X-ray emission from the outflowing hot gas (which was actually detected from such well-known superwind galaxies as M82 (Lehnert et al. 1999) and NGC 253 (Weaver et al. 2002)) and the presence of an optical emission nebula serve as observational manifestations of this phenomenon. In this case, the edge-on orientation of the galaxy is most favorable for the detection of a superwind.

Let us consider the observational evidence suggesting the existence of a superwind in NGC6286 in more detail. According to RASS FSC data, this galaxy is an X-ray source. We detected an optical emission nebula in the galaxy (Figs. 5b and 5c) the size of which reaches ~ 9 kpc in a direction perpendicular to the plane of the stellar disk. Note that the sizes of such nebulae in other superwind galaxies (M 82, NGC 1482, and others) lie within the range from several kpc to several tens of kpc (Heckman et al. 1990). As we noted above, no optical emission is observed inside the cones, because, according to the calculations by Strickland and Stevens (2000), the gas temperature in this region must be $\sim 10^7$ K.

A good illustration of a superwind in a galaxy is an enhanced [NII]6583/H_α the emission-lines ratio compared to an ordinary H II region. Thus, whereas this ratio is ≤ 0.5 in an H II region where photoionization dominates, it is much larger than 0.5 for a supersonic outflow of hot gas and the formation of shock fronts (the conditions under which collisional ionization dominates). We see from Fig. 5f that the derived ratios increase severalfold as one recedes from the disk plane. In this case, the emission-line ratio is highest in the regions that form the boundary of the conical ejections of hot gas from the galactic plane.

The line emission is strongest where the line of sight runs along the walls of the cone. The space velocity here is roughly perpendicular to the line of sight, and the line-of-sight velocities cannot give evidence of such motions. However, the increase in emission lines' $FWHMs$ to $400\,\mathrm{km\,s^{-1}}$ near the walls of the cone and their complex profiles, as was mentioned above, serve as their indirect confirmation.

Thus, we conclude that a superwind-type bipolar outflow of gas from the central region of the disk takes place in the galaxy NGC6286.

We note in passing yet another fact that confirms the interaction between the galaxies. The [NII]λ6583/H_α ratio also increases in the SE part of the galaxy NGC6285 that is closest to NGC6286 (Fig. 5f). This increase may be attributable to the hot superwind gas that heats up and ionizes the interstellar medium in this part of the galaxy, which causes the intensity of the forbidden lines to increase.

Using the typical superwind outflow velocities ($\sim 500\,\mathrm{km\,s^{-1}}$) from Veilleux (2002) and the observed sizes of the ionization region above and under the disk, we can estimate that the ejection began $\sim 10^7$ years ago. This estimate is consistent with the above estimate for the characteristic time of strong interaction.

4. CONCLUSIONS

In conclusion, we emphasize that our kinematics study of the gaseous component of the galaxy NGC6286 has revealed no evidence of gas rotation around its major axis. Therefore, NGC6286 is unlikely to be a galaxy with a forming polar ring, as assumed previously.

Based on the entire set of observational data, we have concluded that the peculiarities of NGC6286 are attributable to the presence of a superwind that outflows from its central region. This is suggested by the following facts:

– the existence of an emission nebula stretching to a distance of ~ 9 kpc from the galactic plane whose shape corresponds to a bipolar outflow of hot gas; the presence of this outflow is confirmed by the presence of an X-ray source;

- the significant increase in [NII]λ6583/H_α ratio characteristic for superwind galaxies;
- the high infrared luminosity of the galaxy, which is indicative of a high star-formation rate ($SFR = 56 - 65\,M_\odot\,yr^1$). The starburst in the central region of the galaxy that gave rise to the superwind was probably triggered by a close encounter of the two galaxies.

Acknowledgements. We are grateful to the Large Telescopes Program Committee for allocating observational time on the 6m telescope and to E.V. Volkov for participation in the discussion of our results. This work was supported in part by the Astronomy Federal Program (project no. 40.022.1.1.1001), the Russian Foundation for Basic Research (project no. 02-02-16033), and the Russian Ministry of Education (project no. E02-11.0-5).

References

Afanasiev V.L., Burenkov A.N., Vlasyuk V.V, & Drabek S.V., Report of SAO RAS, 1995, no. 234
Afanasiev, V.L., Dodonov S.N., & Moiseev A.V., 2001, in "Stellar Dynamics: from Classic to Modern", (Ed. by L. P. Ossipkov and I. I. Nikiforov), St. Petersburg, 103.
Arp H., 1996, ApJS, 14, 1
Baan W.A., 1989, ApJ, 238, 804
Baan W.A., Salzer J.J., & LeWinter R.D., 1989, ApJ, 509, 633
Bosma A., Byun Y., Freeman K.C., & Athanassoula E., 1992, ApJ, 400, L21
Heckman T.M., Armus L., & Miley G.K., 1990, ApJS, 74, 833
Lehnert M.D., Heckman T.M., & Weaver K.A., 1999, ApJ, 523, 575
Moiseev A.V., Bull. SAO, 2001, 51, 11, (astroph/0111219)
Moiseev A.V., Bull. SAO, 2002, 54, 74, (astroph/0211104)
Monnet G., & Simien F., 1977, A&A, 56, 173
Poggianti B.N., & Wu H., 2000, ApJ. 529, 157
Reshetnikov V.P., & Combes F., 1994, A&A, 291, 57
Reshetnikov V.P., Hagen-Thorn V.A., & Yakovleva V.A., 1996, A&A, 314, 729
Sanders D.B., Scoville N.Z., Young J.S., et al., 1986, ApJ, 305, L45
Smith D.A., Herter T., & Haynes M.P., 1996, ApJS, 104, 217
Smith D.A., Herter T., & Haynes M.P., 1998, ApJ, 494, 150
Soifer B.T., Boehmer L., Neugebauer G., & Sanders D.B., 1989, AJ, 98, 766
Soifer B.T., Sanders B.D., Madore B.F., et al., 1987, ApJ, 230, 238
Strickland D.K., & Stevens I.R., 2000, MNRAS, 314, 511
Veilleux S., 2002, in "Galaxies: The Third Dimension", eds. M. Rosada et al, ASP Conf, 282, 293
Veilleux S., Kim D.C., Sanders D.B., et al., 1995, ApJS, 98, 171
Whitmore B.C., Lucas R.A., McElroy D.B., et al., 1990, AJ, 100, 1489
Worthey G., 1994, ApJS, 95, 107
Worthey G., Faber S.M., Gonzalez J.J., & Burstein D., 1994, ApJS, 94, 687
Weaver K.A., Heckman T.M., Strickland D.K., & Dahlem M., 2002, ApJ, 576, L19
Young J.S., Xie S., Kenney J.D.P., & Rice W.L., 1989, ApJS, 70, 699

Translated by V. Astakhov